Humidity response of a capacitive sensor based on auxeticity of carbon nanotube-paper composites

NANO EXPRESS

PAPER

Humidity response of a capacitive sensor based on auxeticity of carbon nanotube-paper composites

Zhongjie Qian[1], **Tianyi Li**[1], **Vigneshwar Sakthivelpathi**[1], **Sheila M Goodman**[2], **Anthony B Dichiara**[2], **Alexander V Mamishev**[3] **and Jae-Hyun Chung**[1]

[1] Department of Mechanical Engineering, University of Washington, Seattle, WA 98195, United States of America
[2] School of Environmental and Forest Sciences, University of Washington, Seattle, WA 98195, United States of America
[3] Electrical and Computer Engineering, University of Washington, Seattle, WA 98195, United States of America

E-mail: jae71@uw.edu

OPEN ACCESS

RECEIVED
14 February 2022

REVISED
10 April 2022

ACCEPTED FOR PUBLICATION
13 April 2022

PUBLISHED
28 April 2022

Keywords: humidity, capacitive, sensor, auxeticity, carbon nanotubes

Supplementary material for this article is available online

Abstract

Auxetic materials showing a negative Poisson's ratio can offer unusual sensing capabilities due to drastic percolation changes. This study presents the capacitive response of wet-fractured carbon nanotube paper composites in exposure to humidity. A strained composite strip is fractured to produce numerous cantilevers consisting of cellulose fibers coated with carbon nanotubes. During stretching, the thin composite buckles in the out-of-plane direction, which causes auxetic behavior to generate the radially structured electrodes. The crossbar junctions forming among the fractured electrodes significantly increase capacitance and its response to humidity as a function of sensor widths. The molecular junctions switch electric characteristics between predominantly resistive- and capacitive elements. The resulting capacitive response is characterized for humidity sensing without the need for an additional absorption medium. The normalized capacitance change ($\Delta C/C_0$) exhibits a sensitivity of 0.225 within the range of 40 $\sim$ 80% relative humidity. The novel auxetic behavior of a water-printed paper-based nanocomposite paves the way for inexpensive humidity and sweat sensors.

1. Introduction

Auxeticity is a structural property showing negative Poisson's ratio. Most materials in nature demonstrate positive Poisson's ratio showing the shrinkage when a material is stretched. However, the auxetic material with negative Poisson's ratio presents expansion under uniaxial tensile force [1]. Auxetic structures such as chiral structure, re-entrant structure, rotating rigid structure [2–4], could be designed for applications to micro devices [5], medical device [6], aerospace [7], and sensors [8, 9]. Other than designed structures, negative Poisson's ratio was frequently observed in fibrous materials [10]. Paper [11] and non-woven fabrics [12] were discovered to possess auxetic behavior. Periodic, repeating structures [13, 14] could be designed to amplify an auxetic effect. One of the auxetic mechanisms in anisotropic paper was the buckling of out-of-plane fibers under a stretched random matrix. Due to buckling, a large negative Poisson's ratio has been observed for individual fibers [15]. The extreme auxeticity enabled the manipulation of out-of-plane electrical junctions for resistance change. While conventional sensors made of a positive Poisson's ratio showed a resistance increase upon pressure, the resistance of an auxetic material decreases due to the recovery of electrical connections [16, 17]. Such a piezoresistive sensitivity was dramatically boosted by forming the junctions made of carbon nanotubes (CNTs).

A carbon nanotube paper composite (CPC) is one of the auxetic materials. In these composites, CNTs deliver electrical conductivity, while cellulose fibers offer the structural frame [18]. Since cellulose fibers are the structural component of a composite, the deformation of cellulose fibers contributes to the auxetic behavior under stretching. In our previous research, the auxetic behavior of CPC has been characterized for elastic and plastic regions [19]. To better control the fracture process, water was printed through a capillary nozzle to initiate the dissociation of cellulose fibers. CPC could be cracked and fractured at a water-printed region. The

auxeticity of the water-printed CPC was pronounced due to the stress concentration of varying elasticity and Poisson's ratio in the dry-wet-dry CPC regions. The uniformly cracked and fractured CPC showed a remarkable resistive sensitivity due to the rapid percolation change under pressure.

A designed auxetic structure has been studied to enhance the capacitive strain sensitivity [9]. The capacitive sensitivity of fractured CPC to humidity is yet to be discovered. We hypothesize that water molecules introduced to the conductive fibrous junctions can modify capacitive characteristics in conjunction with auxeticity. To test the hypothesis, this study investigates the capacitive sensitivity to water vapors for various widths of CPC fractured by a wet-stretching method. The capacitive response to humidity is investigated in terms of strain, Poisson's ratio, and CPC widths. As a practical application, humidity and sweat sensing capability is demonstrated.

2. Experimental methods

2.1. CPC preparation

CNT-cellulose composite papers were prepared following a modified TAPPI T-205 standard method [20]. In short, hydroxyl-functionalized multiwalled carbon nanotubes (MWCNTs) were dispersed in a binary mixture of alkali lignin (AL, 99%) and sodium dodecyl sulfate (SDS; 90:10 wt) [21]. The aqueous dispersion of CPAM was first added to pulp fiber solutions (0.3% consistency) and combined on a hot plate at 50 °C for 30 min. The as-dispersed CNT-OH solutions were then added to the pulp mixture. The combined CNT-OH and pulp suspensions were then filtered, pressed, and dried to form hand sheets. The CNT concentration in CPC was 10 wt%.

2.2. Fabrication of the CPC piezoresistive sensors by water-printing

CPC capacitive sensors were fabricated by controlled water-printing and axial stretching (figure 1(a)) [19]. A 100 μm-thick CPC strip was trimmed to make a 20 mm-long strip. The strip widths of 1, 3, 5, 7, and 10 mm were prepared. Silver paste (MG Chemicals, USA) was applied to both ends of a CPC strip and cured at 70 °C on a hot plate to make electrodes. Using a 0.7 mm-diameter capillary pen, water was printed along the centerline without physical contact with CPC.

To test the auxetic behavior, a tensile testing stage with a uniaxial actuator was constructed. The tension was applied with a constant speed of 38 μm s^{-1} (supplementary information, Wet_fracture_method.mp4 (available online at stacks.iop.org/NANOX/3/025001/mmedia)). To study the auxetic effect of CPC to humidity, humid air was directly supplied to a CPC specimen through a 12 mm-diameter nozzle in a tensile test. Both force and resistance were measured by a load cell (DYMH-103, CALT, China) and a high impedance multimeter (Fluke Corp., USA, Fluke 287), respectively. The stress was calculated by $\sigma = \frac{F}{d_0 \times \mathrm{th}}$, where F was the force measured by the load cell, d_0 was the initial width of a specimen, and th was the initial thickness (i.e., 100 μm) of the specimen. The axial strain was defined as $\varepsilon = \frac{l - l_0}{l_0}$. CPC specimens without water-printing were also tested to compare auxeticity and capacitive change with water printing.

2.3. Auxetic behavior characterization

To investigate the width effect on auxeticity with respect to capacitance, specimen widths of 1, 3, 5, 7, and 10 mm were prepared. The auxetic behavior was studied by measuring the thickness changes. In the testing stage (figure 1(a)), a microscope was focused on the water-printed region of the specimen from the top- and side views (x-y and x-z planes). The thickness change of a specimen in water-printing and stretching was measured. The effective Poisson's ratio was computed at the maximum thickness by the following equation:

$$\nu_{eff} = -\frac{(z_i - z_0)/z_0}{(l_i - l_0)/l_0} \tag{1}$$

where z_i and l_i denoted the specimen thickness and length at a given strain level, and z_0 and l_0 denoted the original specimen length and thickness. For both specimens with and without the water-printing, ν_{eff} was computed at strain ranging $0 \sim 0.36$.

2.4. Characterization of fractured CPC

Scanning electron microscopy (SEM, XL830, FEI Company, Hillsboro, OR, USA) was used to study the in-plane and cross-section morphology of water-printed CPC stretched at various strain levels. To ascertain the fracture length and morphology, the CPC was mounted to a flat aluminum stage using double-sided carbon tape and imaged using a 5 kV accelerating voltage with a 5 mm working distance.

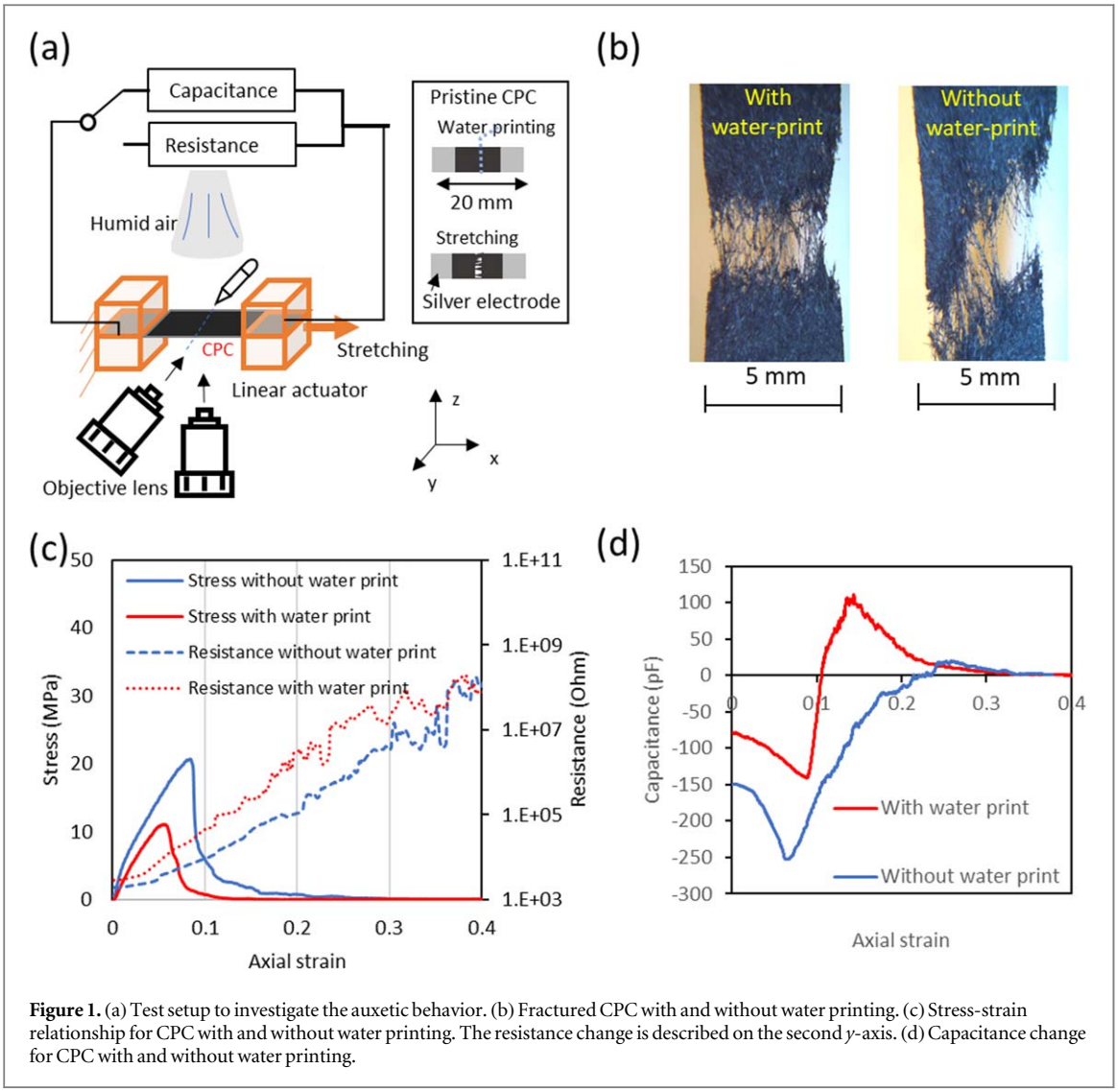

Figure 1. (a) Test setup to investigate the auxetic behavior. (b) Fractured CPC with and without water printing. (c) Stress-strain relationship for CPC with and without water printing. The resistance change is described on the second *y*-axis. (d) Capacitance change for CPC with and without water printing.

2.5. Characterization of resistive and capacitive changes for humidity

Humidity-induced resistive and capacitive changes were studied for CPC sensors prepared at various strain levels of 0.10, 0.12, 0.15, 0.18, and 0.24. The specimens were placed at 35% relative humidity (RH) for the first 20 s before supplying humid air. Note that a humidity chamber was not used in this test. Instead, humid air was directly supplied to a CPC specimen with 10 mm-distance for 50 s. Subsequently, humid air was removed to leave the sensor at 30% RH for 110 s. Therefore, the total time of the experiment for each specimen was 180 s. The capacitance values were measured by a capacitance meter (GLK instruments 3000). The experiment was also repeated for resistive measurement (Fluke-287). Meanwhile, a commercial humidity sensor (DHT11-Temperature and Humidity Sensor) was located next to a CPC specimen for comparison.

2.6. Cyclic humidity test for a capacitive sensor

CPC specimen (5 mm width) with 0.24-strain were placed into a 3.8 l-chamber equipped with a humidifier and a vacuum pump. The humidity inside the chamber was monitored at a rate of 1 sample/s using a resistive humidity sensor (DHT11). Cyclic experiments were conducted by varying the humidity within the RH-37 $\sim$ 100% for 10 cycles. The evolution of the CPC capacitance values as a function of RH was recorded in real-time using a capacitance meter (GLK 3000). Also, six more sensors were fabricated to test the reproducibility.

To investigate the humidity sensing mechanism of a fractured CPC sensor, four different CPC sensors and one aluminum sensor were prepared (table 1). The four different CPC sensors were fractured CPC sensor prepared by 0.24-strain, a fractured sensor coated with polyacrylic acid (1%–PAA), a fractured CPC sensor laminated with a 20 μm-thick polyester film, and a CPC sensor trimmed with scissors without fracture. An aluminum sensor was prepared by trimming a 100 μm-thick aluminum foil. All the surface area of one electrode was 5 $\times$ 5 mm^2.

Table 1. Summary of the prepared humidity sensors.

Sensor material	0.24-strain	Scissor trimming	Coating	Area (mm^2)/thickness (mm)
Fractured CPC	Yes	No	No	5 × 5/0.1
PAA-coated fractured CPC	Yes	No	1%-PAA	5 × 5/0.1
PET-laminated fractured CPC	Yes	No	PET film	5 × 5/0.1
Trimmed CPC	N/A	Yes	No	5 × 5/0.1
Trimmed Aluminum foil	N/A	Yes	No	5 × 5/0.1

The PAA-coated CPC was prepared to study if the swelling ability of cellulose fibers could enhance the capacitive sensitivity. A 1%–PAA-solution was deposited into a CPC sensor and cured on a hot plate (100 °C) for one h. After curing, the sensor was fractured by introducing 0.24-strain. A fractured CPC sensor laminated with a polyethylene terephthalate (PET) film was used to test a sensitivity without direct contact of CPC to humidity. In comparison to a fractured CPC sensor without lamination, the response of a laminated sensor could give insight about the sensing mechanism: whether the sensitivity resulted from the cantilever-shaped electrodes or the CNT surface change. A scissor-trimmed CPC sensor was used to study a sensitivity without cantilever-shaped electrodes. Scissor-trimmed aluminium electrodes were fabricated in the same way as scissor-trimmed CPC electrodes. A scissor-trimmed aluminium capacitance was prepared to study the CNT surface change in comparison to the aluminium surface.

3. Results and discussion

3.1. Capacitive and resistive characterization of CPC sensors by water-printing and stretching

The CPC sensors were fractured under a water-printed condition using the setup (figure 1(a), supplementary information: wet_fracture_method.mp4). To study the capacitive and resistive changes in coupling with the auxeticity, three CPC sensors were stretched with and without water printing. Optical microscopes were placed to observe the top views of the fracture process (figure 1(b)). From the images, the CPC samples without and with water printing were clearly differentiated. The crack of the water-printed sensor was created along the waterline, perpendicular to the stretching direction. The crack of the CPC without water printing was propagated at a 45-degree angle to the stretching direction due to shear failure. Figure 1(c) shows the stress-strain relationship for CPC with and without water printing. The strength for a water-printed CPC was lower than that of a CPC without water printing. The resistance increased by a power law due to the rapid increase of percolation.

The capacitive response of the CPC sensors with and without water printing was measured under the RH-100% condition (figure 1(d)). The nozzle connected to a humidifier was applied directly on the specimen surface in stretching. The capacitance of the specimens with and without water printing started with negative values because the produced capacitance was connected in parallel with the electrical resistance. The negative capacitance was caused by the leakage of electric current through a resistive connection of CPC. As a CPC specimen started to fracture, the negative capacitance magnitude increased. Note that the dip in the negative capacitance was the characteristic of a capacitance meter circuit, not the characteristic of a CPC specimen. According to our characterization of the capacitance meter, as the resistance increased, the negative capacitance magnitude showed a dip followed by a continuous increase to 0 pF. As the strain crossed 0.1, the capacitance of water-printed CPC became positive, while the CPC capacitance without water-printing was negative at 0.1-strain. Interestingly, the CPC capacitance with water-printing reached the maximum value of 103.3 pF and converged to 0 pF as the distance between two fractured CPC electrodes increased. The two capacitance curves met at 0.24-strain, where the samples were completely terminated electrically and mechanically.

Figures 2(a) and (b) show the SEM images of the cross-section for 5 mm-wide specimens at 0.12 and 0.18 strains, respectively. In comparison to the thickness of the specimen without water-printing, the thickness increase of a water-printed specimen was greater (figure 2(c)). The thickness increase of a water-printed specimen reached the maximum value when the applied strain was 0.24. As the specimen was completely fractured, the thickness increase stopped with the complete release of a tension.

The width increase of water-printed specimens enhanced the auxeticity, which increased the magnitude of Poisson's ratio (figure 2(d)). When the width increased from 1 to 10 mm, the capacitance increase was proportional to the widths between 3 and 10 mm after applying the same 0.24 strain (figure 2(e)). Since the specimen was stretched under RH-100%, the relationship between sample widths and capacitances demonstrated the sensitivity to humidity. In the graph, a 1 mm-specimen showed the smaller capacitance value than the linear equation given in figure 2(e). The smaller capacitance at a 1 mm-specimen resulted from the smaller Poisson's ratio as shown in figure 2(d). In comparison to the capacitance made of a trimmed aluminum

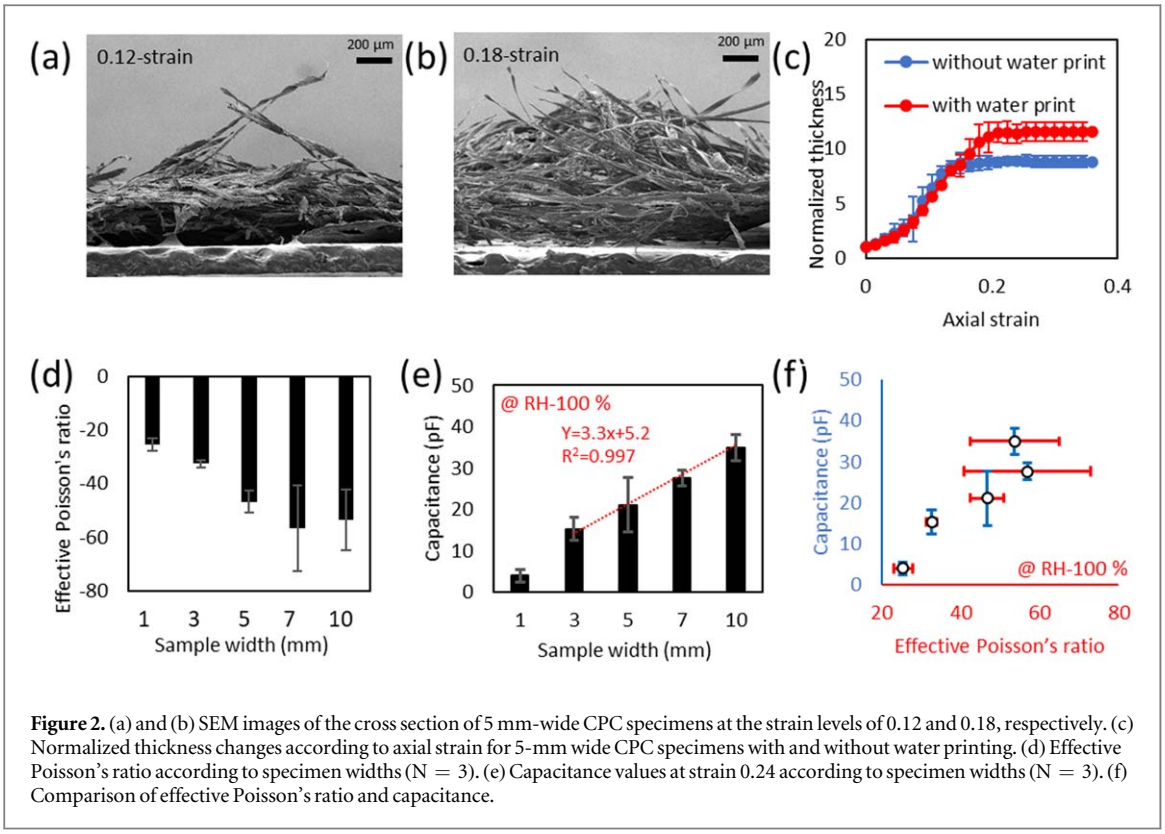

Figure 2. (a) and (b) SEM images of the cross section of 5 mm-wide CPC specimens at the strain levels of 0.12 and 0.18, respectively. (c) Normalized thickness changes according to axial strain for 5-mm wide CPC specimens with and without water printing. (d) Effective Poisson's ratio according to specimen widths (N = 3). (e) Capacitance values at strain 0.24 according to specimen widths (N = 3). (f) Comparison of effective Poisson's ratio and capacitance.

film having the widths between 1 and 10 mm, the CPC capacitance was 41.2 times (supplementary information, figure S1). The fibrous junctions produced by auxeticity evidently increased the capacitance.

Figure 2(f) shows the comparison between Poisson's ratio and capacitance. At the smaller widths of a specimen, the capacitance increased as the Poisson's ratio increased. Since the Poisson's ratio saturated for the specimen wider than 3 mm, the capacitance increase was only dependent on the width increase.

To analyze the reason of the auxeticity increase due to the width, numerical simulation was conducted using COMSOL Multiphysics. A 1-mm displacement was applied on the right end at the longitudinal direction to simulate the tensile deformation (supplementary information, figure S2). Because of the positive x-y Poisson's ratio, compressive stress was generated at the wet region across the central line along the y-direction (figures 3(a)–(c)).

The average compressive stress was then compared with the stress from the critical buckling force under the pin-joint conditions, which was described as:

$$P_{cr} = \pi^2 EI/L^2 \tag{2}$$

where I is the moment of inertia, E is the Young's modulus in the wet region, and L is the width of a CPC strip. Critical buckling stress was obtained by dividing P_{cr} with the cross-sectional area (thickness x width). According to the numerical results (figure 3(d)), the compressive stress could cause the buckling of a specimen wider than 1.9 mm. Over the critical width, the CPC specimen could buckle due to the increased aspect ratio (width/thickness = 19). The buckling increased the Poisson's ratio and auxeticity. The numerical results agreed with the experimental results. When the width was greater than 3 mm, the CPC specimen could be buckled with a periodicity (supplementary information, figure S3), which could reduce the thickness increase. As a result, the capacitance increase was proportional to the width for the specimens wider than 3 mm.

3.2. Characterization of resistive and capacitive changes for humidity

To investigate the resistive and capacitive changes to humidity for various axial strains, the CPC samples with the applied strain of 0.1, 0.12. 0.15, 0.18, and 0.24 were exposed to RH-35 ~ 100% (25 °C). The 0.1-strain was an initial value because a positive capacitance value was measured for a water-printed CPC specimen. According to the programmed humidity in figure 4(a), both resistive and capacitive changes were measured (figures 4(b)–(f)). For the CPC with 0.10, 0.l2, and 0.15, the resistance gradually increased as the humid air was supplied and reached a plateau at 50 s. When the humid air was removed at 70 s, the resistance increased again. As the applied strain was greater, the duration time of the increasing resistance value expanded. Under humid air, the resistance increase was originated from the swelling of fibers coated with MWCNTs due to water molecules. The

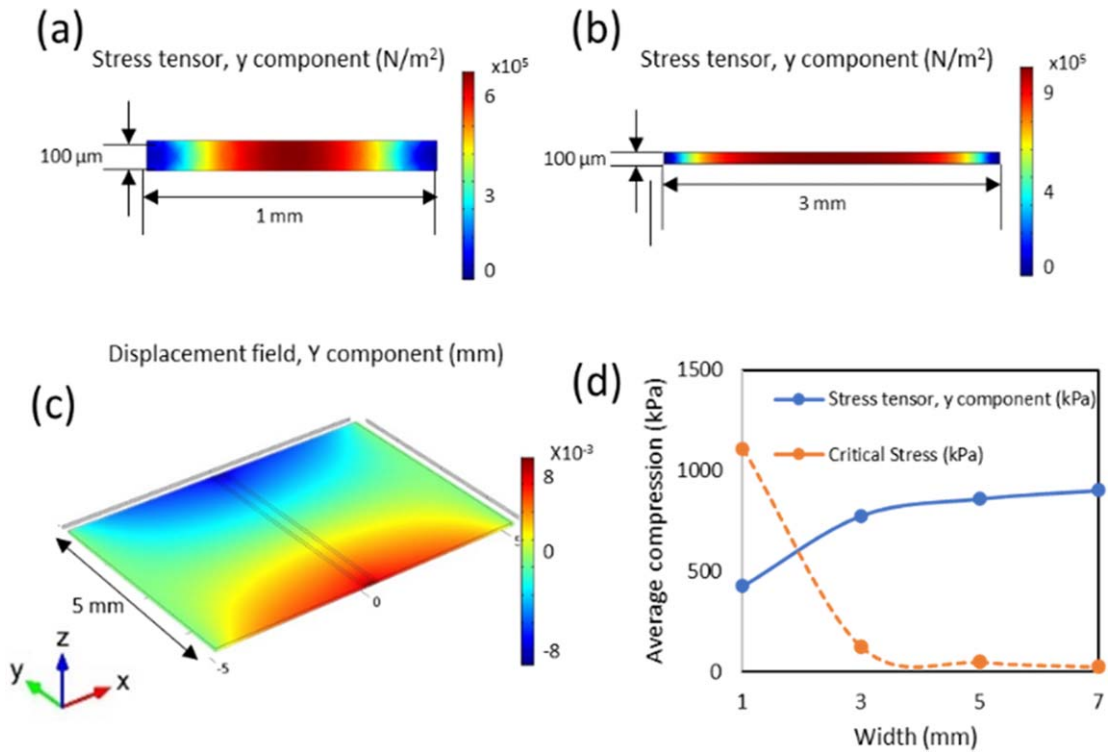

Figure 3. (a) Stress distribution on a 1-mm wide-CPC specimen. (b) Stress distribution on a 3-mm wide specimen. (c) Compressive stress is built across the width of a 5-mm wide specimen. (d) Comparison of average compressive stresses and critical buckling stresses according to specimen widths.

hydroexpansion of cellulose fibers enlarged the distance between CNTs and broke the percolation network, which prevented electrical interactions among CNTs, therefore increasing the composite resistance [22]. In our experiment, the resistance change was even greater because the auxeticity at fracture produced a greater water absorption through the larger surface area. Although humid air was removed at 70 s, plenty of water molecules were absorbed, and part of them were left in the fibers. With the larger expansion, we observed a longer time of the second leap of the resistance increase.

The reason for the second leap was that, as the larger an axial strain was applied, the more surface area was generated because of the auxeticity. The longer time of resistance rise was achieved by swelling due to the extra amount of absorbed water molecules. Notably, it was found that the resistance values suddenly increased or decreased due to the fragile molecular junctions created by the broken fibers. The exposed fibers behaved as compliant cantilevers, which were extremely sensitive to environmental intervention, including humidity, pressure, and airflow. When the high intensity of humid air was supplied, the structure and shape of the fiber network in the crack domain could be changed abruptly to increase the resistance for the samples with 0.12, 0.15, and 0.18 strain.

For the CPC with 0.24-strain, the specimen showed extreme binary characteristics between capacitance and resistance (figure 4(f)). At this strain, the resistance was infinite, but the capacitance was generated among very closely located fibers. For plotting purposes, the beginning point of resistance was set as 500 MΩ, which was the maximum measurable resistance. Upon exposure to humidity, the resistance value decreased from infinity to a few MΩ because of water molecules trapped between fibers. A direct electric current flowed through water molecules upon humidity exposure. Without humid air, the junctions were not connected and behaved as a pure capacitor. According to the square input of RH-35 $\sim$ 100% humidity, the response time was 3s and the recovery time was 83s (supplementary information, figure S4).

For the CPC samples at each strain, the capacitance showed a relatively smooth transition. As soon as humid air was supplied, the capacitance increased. When humid air was removed, the rising trend was instantly changed to a descending trend. Sometimes, a sudden capacitance drop was shown due to a temporary electrical connection with water vapor. Note that the capacitance values for all the samples changed in a similar fashion but with different magnitude. The magnitude of the capacitance change due to humidity decreased with the larger axial strain. The peak values of capacitance were 2.98, 3.94, 2.22, 0.88, and 0.45 pF for the CPC specimen

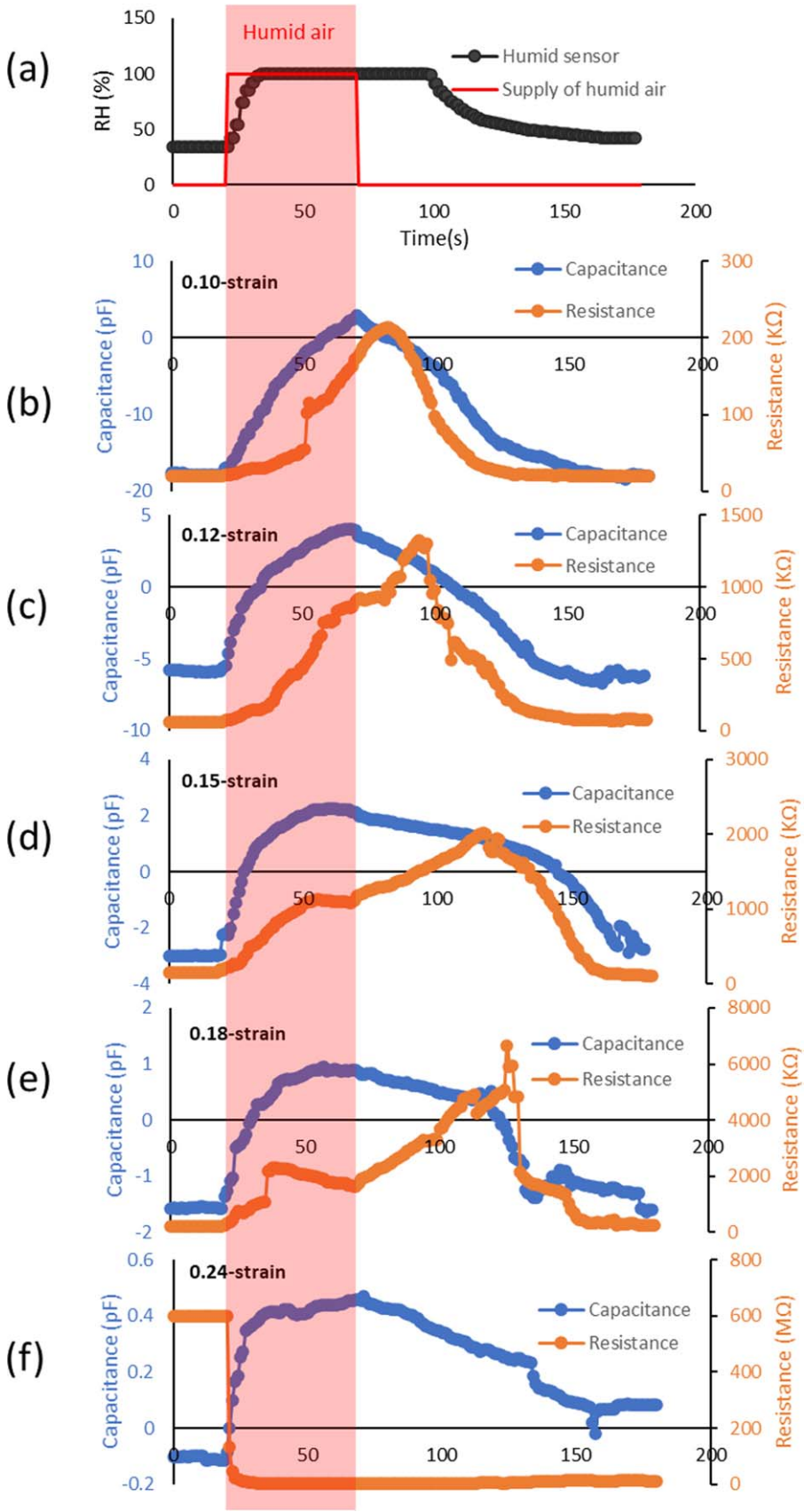

Figure 4. (a) Programmed humid air and detected humidity change. (b) ∼ (f) Capacitive and resistive characteristics for CPC specimens with 0.1, 0.12. 0.15, 0.18, and 0.24-strains.

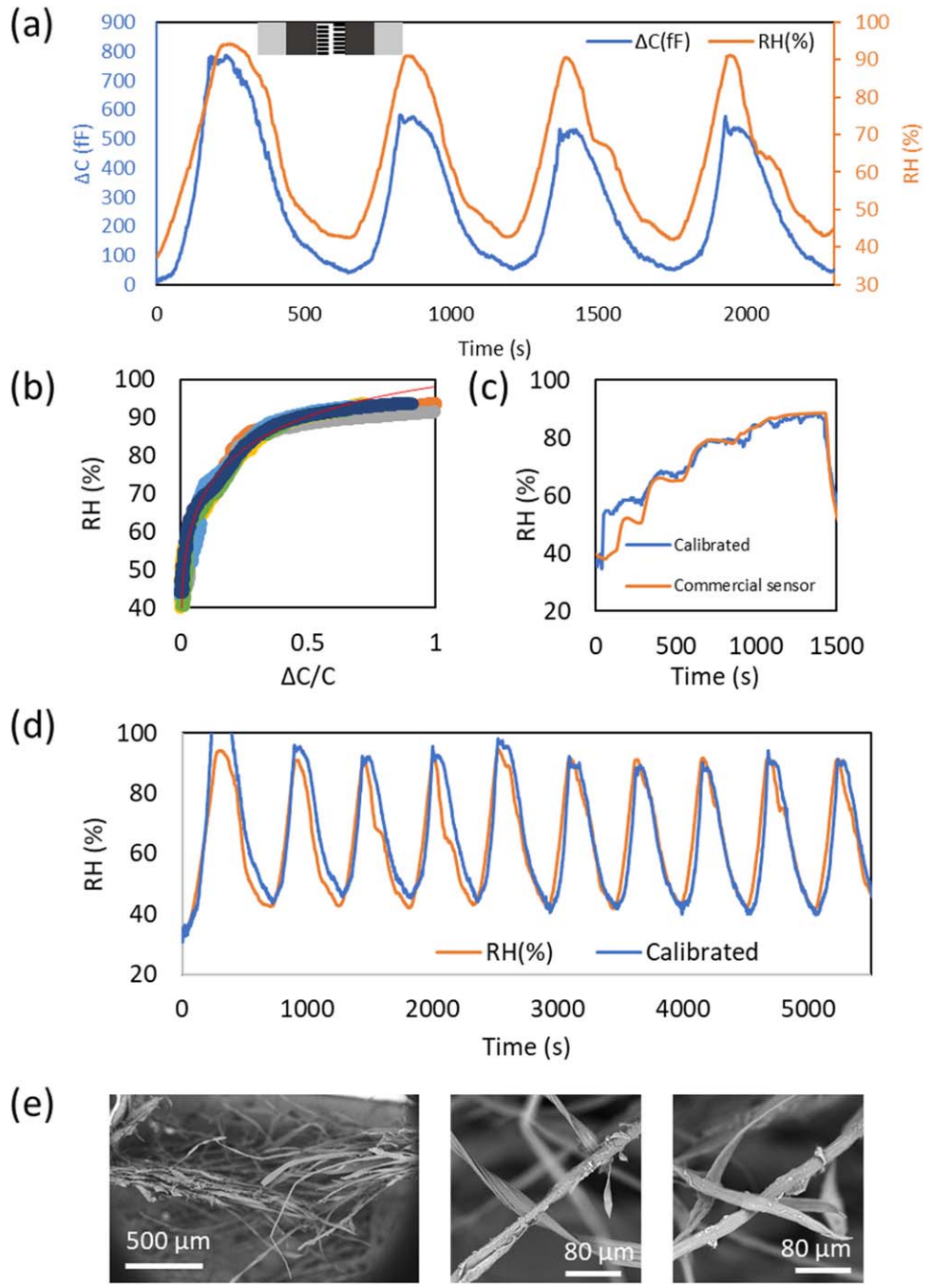

Figure 5. (a) Capacitance change of a fractured CPC sensor according to cyclic humidity change. The 5mm-wide CPC sensor is made of 0.24-strain. (b) Relationship between RH and $\Delta C/C_0$ (N = 6). the red line shows the empirical equation. (c) Comparison of a CPC sensor response to a commercial sensor response for the staircase input of humidity. (d) Comparison of a calibrated CPC-humidity response to a commercial sensor for 10 cycles. (e) SEM images for a CPC sensor fractured with 0.24 strain. molecular crossing junctions to detect humidity without absorption medium.

with 0.1, 0.12, 0.15, 0.18, and 0.24-strains, respectively. The highest capacitive sensitivity of the CPC sensor was at the 0.12-strain, which was right after a fracture.

3.3. Cyclic humidity test for a capacitive sensor

Figure 5(a) shows the capacitance change for a CPC humidity sensor for the first four cycles of RH 40 $\sim$ 90%. Except for the first cycle, the measured capacitance values were stable and reproducible. The normalized capacitance change ($\Delta C/C_0$) at the tested RH was 0.47 $\pm$ 0.03. During the humidity test, the temperature change was less than 1 °C (supplementary information, figure S5). The capacitive change due to the temperature change could be neglected.

Table 2. Comparison of capacitive humidity sensors.

	$\Delta C/C_0$ (RH 40 ~ 80%)	Electrodes and dielectric medium
CPC	0.225	Electrode: fractured CPC (0.24 strain), medium: none
[23]	0.15	Electrode: metal, medium: bis(benzo cyclobutene)
[24]	0.10	Electrode: Au film, medium: carbon black polyimide
[25]	0.09	Electrode: Aluminum, medium: polyimide
[26]	0.05	Electrode: Au layer, medium: polyimide
[28]	0.015	Electrode: interdigitated textile electrodes, medium: metal-organic framework layer
[29]	0.25 RH 40%–65% 75 RH 65%–85%	Electrode: Interdigitated electrodes, medium: crystalline trianglamine hydrochloride
[30]	350	Electrode: coplanar interdigitated electrodes, medium: nanostructured TiO_2 thin films
[27]	0.5	Electrode: aluminum layer, medium: $Cu_3(BTC)_2$ film
[34]	0.08	Electrode: printed silver, medium: Ag electroplating with Ni or parylene-C
[31]	1.8	Electrode: inkjet-printed interdigitated silver, medium: paper (cellulose fibers)
[32]	0.04	Electrode: copper, medium: graphene oxide-coated silk fiber
[33]	0.016	Electrode: copper, medium: graphene in polyvinylidene fluoride

Figure 5(b) shows the normalized capacitance change ($\Delta C/C_0$) for the cyclic test of RH 40 ~ 90% (N = 6). Based on the graph, the empirical equation ($r^2 = 0.93$) between the normalized capacitance value and the relative humidity was:

$$RH = 106.6x^{0.1778} - 6x \tag{3}$$

where x is the normalized capacitance value ($\Delta C/C_0$).

When a staircase input of humidity was given, the response was similar to that of a commercial sensor (DHT11) (figure 5(c)). The CPC sensor gave a more rapid response to the humidity change at the beginning and followed the similar trend to a commercial sensor.

In comparison to other capacitive humidity sensors, the normalized capacitance changes ($\Delta C/C_0$) at RH-40 ~ 80% are summarized with the electrode and medium materials in table 2. Most capacitive humidity sensors were fabricated in the form of a dielectric layer between two electrodes. Dielectric materials and electrode surfaces were modified to enhance sensitivity. Also, interdigitated electrodes (IDE), porous materials, and nanomaterials contributed to sensitivity improvement. For the modification of a dielectric medium [23–26], the sensitivity was linear with a relatively small change of $\Delta C/C_0$. Thin-film coating [27] on electrodes could drastically increase the capacitance change when RH was elevated because of the higher water absorption. When IDE was used with an additional coating material [28–30], the sensitivity increased nonlinearly. Inkjet-printed IDE on paper substrate [31] showed a linear response to humidity but with a delayed response time of 250 s at RH-40 ~ 100%. A capacitive humidity sensor with a modified hydrophobic dielectric material showed a humidity response [32, 33]. In summary, our CPC sensor showed a relatively higher $\Delta C/C_0$ of 0.225 at RH-40 ~ 80%. Since our sensor did not require an absorption medium, the fabrication process using a tensional fracture was simple and rapid.

Figure 5(d) shows the comparison between the calibrated RH data of a CPC sensor using equation (3) and that by the reference humidity sensor, which showed a good agreement. Also, six additional sensors were tested for four humidity cycles in order to evaluate the reproducibility (supplementary information, figure S6). For the measurement obtained after the initial cycle, the sensor response became repeatable and stable.

The high capacitive sensitivity of the fractured CPC composite to the humidity resulted from the molecular junctions made by the large auxetic behavior. The major contribution of auxetic behavior was to form the molecular junctions among radial crossing structures (figure 5(e)), which produced an extreme capacitive sensitivity to humidity. The molecular junctions were newly generated capacitance from the randomly oriented fiber network through water printing and wetting. When the junctions were exposed to water vapor, the water molecules adsorbed at the junctions worked as the media with high permittivity. At the larger strain values, the gap between fibers increased, hence reducing the sensitivity. For example, when the molecular junctions were eliminated with a 1 mm distance between the electrodes, the high sensitivity to humidity disappeared.

To elucidate the capacitive sensing mechanism of humidity, three more CPC sensors were prepared as shown in table 1; CPC sensors coated with PAA, a polyester film, and trimmed with a scissor. A metallic capacitive sensor was also prepared by trimming a 100 μm-thick aluminum foil with the same dimensions. Figure 6(a) shows the capacitance change of a fractured CPC coated with PAA. The PAA-coated CPC sensor showed the multistage swelling effect. When contacting with water vapor, both PAA and fibers could swell with hydroexpansion, which showed the phase shift. The magnitude of capacitance change was ~100 fF, which was much smaller than the CPC sensors without PAA coating. The hysteresis potentially caused by the swelling effect

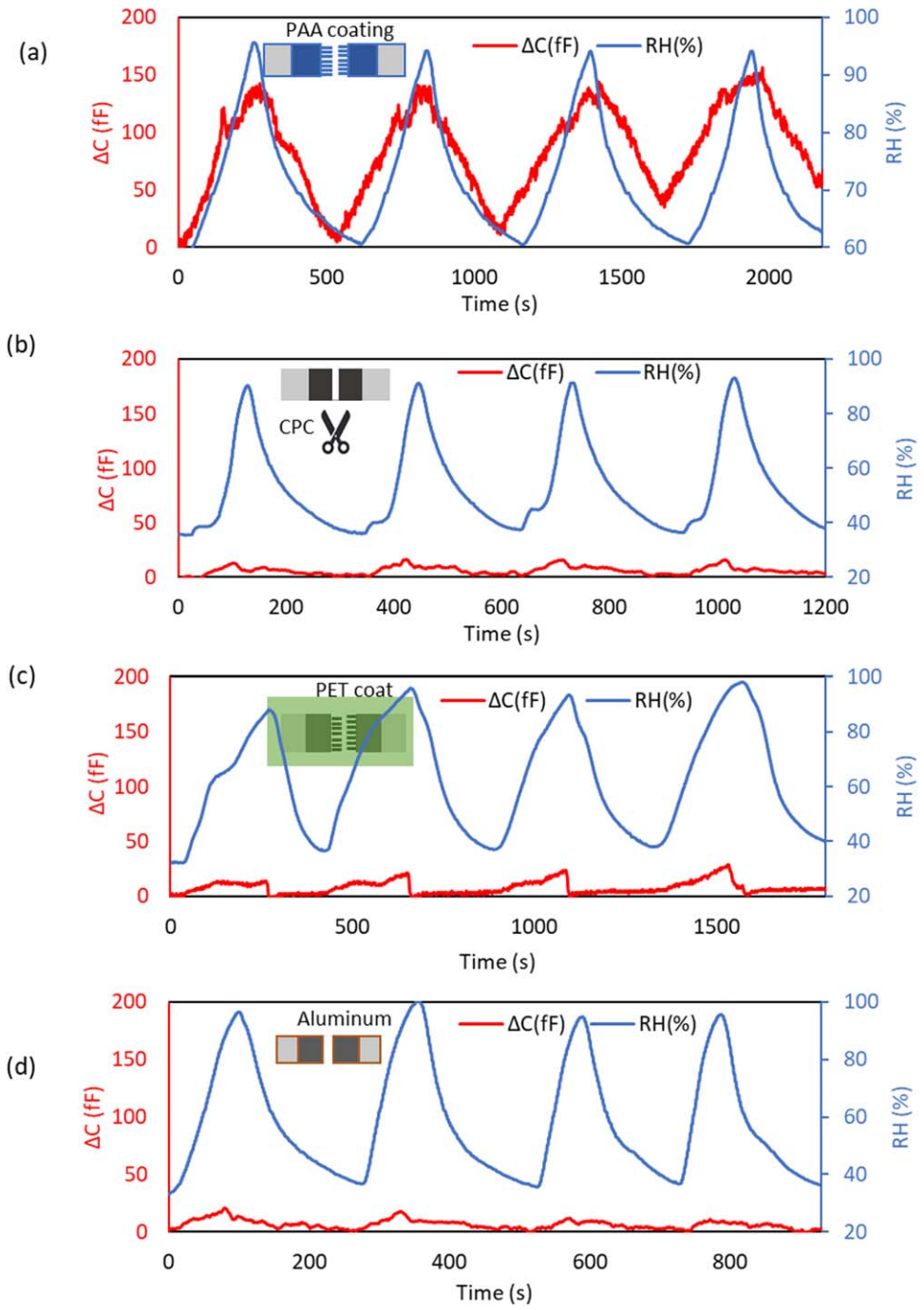

Figure 6. Capacitive changes of (a) PAA-coated fractured CPC, (b) trimmed-CPC, (c) PET film-coated fractured CPC, and (d) trimmed aluminum sensors for cyclic humidity change.

became greater to reduce the capacitive change for repeated cycles. Therefore, the capacitive response of fractured CPC was not originated from the swelling effect but could be resulted from the capacitive change on the MWCNT surface of the fractured fibers.

A scissor-trimmed CPC sensor without fracture (figure 6(b)) showed a change of 10 fF in the given humidity range. The fractured CPC coated with a PET film showed a change of 20 fF because the water adsorption was blocked by a plastic film (figure 6(c)). The sensitivity was higher than that of a trimmed CPC sensor due to the higher electric field strength and the larger surface area generated by the high aspect ratio CNT-coated fibers. The metallic capacitive sensor showed a 10 fF change similar to the trimmed CPC sensor (figure 6(d)).

For humidity sensing, resistive and capacitive sensors are commercially available. Between two electrodes, a humidity absorption pad is applied to change resistance or capacitance. Using CNTs, a humidity sensor was investigated for a resistive sensor due to the changes in the absorption of water molecules [35]. The resistance change of CPC coated with PAA was also sensitive to humidity due to a swelling effect [36, 37]. The fractured

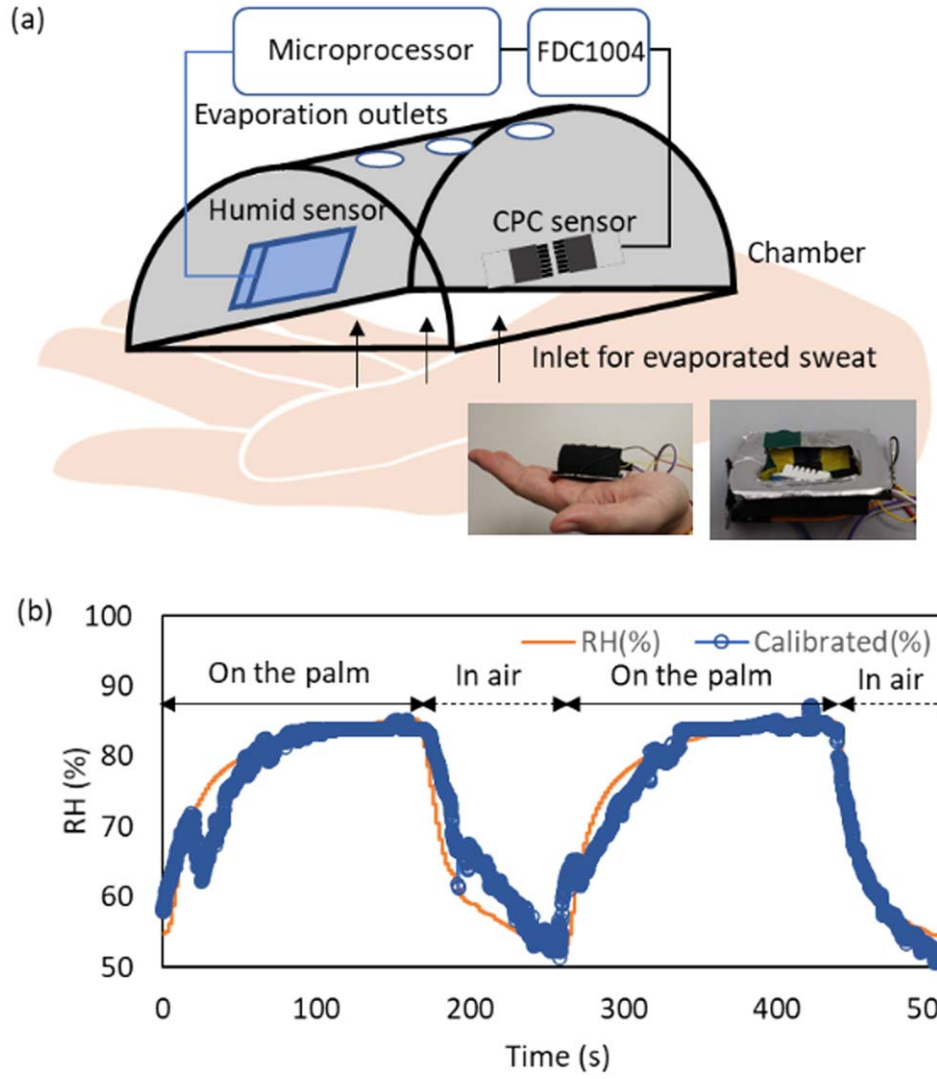

Figure 7. (a) Chamber to measure humidity change on a hand. A commercial humidity sensor is integrated with a fractured CPC sensor. To eliminate the parasitic capacitance from the human hand, the chamber is covered with an electrically grounded aluminium foil. The test has been conducted multiple times only for one subject. (b) Capacitance change is measured on the palm and in the air. The humidity change of a capacitive CPC sensor shows a good agreement with that of a resistive commercial sensor. The study related to sweat monitoring was approved by the institutional review board (IRB) at the University of Washington (IRB ID: STUDY00010741). The sensor characterization has been conducted according to the approved procedure under the consent of the study participant.

CPC capacitive sensor was novel in that the capacitive change to humidity was significant without a dielectric medium. A capacitive sensor using air as a medium did not function due to negligible permittivity change of air. The high electric field and the large surface area contributed to the sensitive measurement to humidity. When the fractured fibers coated with CNTs were blocked with a polyester film, the humidity change was still detectable but had a reduced sensitivity. The experimental results showed that the major capacitive response resulted from the change of CNT surface on cellulose fibers. The molecular junctions of a fractured CPC sensor created the significant capacitance change without a dielectric medium, which facilitated a highly sensitive capacitive sensor as shown in table 2.

3.4. Application to sweat sensing

A fractured CPC sensor with 0.24-strain could be used to evaluate the sweat evaporation of a human's skin. To test a CPC sensor, a small chamber with an evaporation hole to contain a commercial humidity sensor and a CPC sensor was constructed (figure 7(a)). When a CPC sensor was placed in the center of the palm, sweat evaporation was detected from a human hand. The data obtained from a CPC sensor were measured using a capacitance-to-digital chip (FDC1004) that was controlled by a microprocessor (Atmega 328). When the chamber was placed on the palm, the RH reached 85%. The RH decreased to 55%, when the sensor was removed

from the palm. The calibrated humidity data for CPC were compared to those of a commercial sensor (figure 7(b)). The calibrated data showed a good agreement with the reference commercial sensor. In the experiment, the sensor chamber was grounded with an aluminum foil to avoid the interference from the human body and other environmental noises. Using the electrically isolated chamber, the selectivity to humidity could be obtained.

4. Conclusions

The capacitive sensing mechanism of an auxetic CPC composite was investigated under varying humidity conditions. When a water-printed CPC composite was stretched, the auxetic behavior produced the radial structures of cellulose fibers embedded with MWCNTs. The high aspect ratio fibers of fractured CPC generated crossing junctions at the crack of the water-printed region. Water molecules introduced on the surface of the crossing radial structure enlarged the capacitance change among the high aspect ratio electrodes, resulting in the extreme change of capacitance. The normalized capacitance change ($\Delta C/C_0$) for a CPC humid sensor was 0.225 in the relative humidity ranging 40 $\sim$ 80%. Since the auxetic behavior was enlarged with the buckling on the out-of-plane direction of a CPC composite, the larger width generated a 40 times-capacitance in comparison to the capacitance of the planar metal electrodes of the same dimensions. According to our further analysis, the capacitive sensitivity to humidity was originated from the molecular junctions of the crossing conductive fibers that trapped water molecules. Due to the molecular junctions, a large change of capacitance could be obtained without a humidity absorption medium. An empirical equation between capacitance and RH was obtained by calibration with a reference humidity sensor. The CPC-capacitive sensor could be used for sweating measurements on the hand. The auxetically produced capacitive sensing platform can facilitate a wearable sensor measuring humidity and sweat.

Acknowledgments

The authors acknowledge the support from the Advanced Manufacturing Program of National Science Foundation (No. 1927623). ZQ, ABD, and JC acknowledge the partial support from IP group and Somalytics. The study related to sweat monitoring was approved by the institutional review board (IRB) at the University of Washington (IRB ID: STUDY00010741).

Data availability statement

All data that support the findings of this study are included within the article (and any supplementary files).

ORCID iDs

Jae-Hyun Chung https://orcid.org/0000-0002-9861-8559

References

[1] Wang Z, Luan C, Liao G, Liu J, Yao X and Fu J 2020 Progress in auxetic mechanical metamaterials: structures, characteristics, manufacturing methods, and applications *Adv. Eng. Mater.* **22** 2000312
[2] Wu W W, Hu W X, Qian G A, Liao H T, Xu X Y and Berto F 2019 Mechanical design and multifunctional applications of chiral mechanical metamaterials: a review *Mater. Des.* **180** 107950
[3] Almgren R F 1985 An isotropic 3-dimensional structure with poisson ratio $= -1$ *J. Elast.* **15** 427–30
[4] Grima J N and Evans K E 2000 Auxetic behavior from rotating squares *J. Mater. Sci. Lett.* **19** 1563–5
[5] Zega V, Nastro A, Ferrari M, Ardito R, Ferrari V and Corigliano A 2019 Design, fabrication and experimental validation of a MEMS periodic auxetic structure *Smart Mater. Struct.* **28** 095011
[6] Evans K E and Alderson A 2000 Auxetic materials: functional materials and structures from lateral thinking! *Adv.* **12** 617
[7] Li D C *et al* 2018 A review of modelling and analysis of morphing wings *Prog. Aerosp. Sci.* **100** 46–62
[8] Trung T Q and Lee N E 2016 Flexible and stretchable physical sensor integrated platforms for wearable human-activity monitoring and personal healthcare *Adv.* **28** 4338–72
[9] Shintake J, Nagai T and Ogishima K 2019 Sensitivity improvement of highly stretchable capacitive strain sensors by hierarchical auxetic structures *Front. Robot. AI.* **6**
[10] Peng R, Ma Y D, Wu Q, Huang B B and Dai Y 2019 Two-dimensional materials with intrinsic auxeticity: progress and perspectives *Nanoscale.* **11** 11413–28
[11] Stenberg N and Fellers C 2002 Out-of-plane poisson's ratios of paper and paperboard. nord. pulp pap *Res. J.* **17** 387–94
[12] Thirlwell B E and Treloar L R G 1965 Non-woven fabrics: VI. Dimensional and mechanical anisotropy *Text. Res. J.* **35** 827–35
[13] Dirrenberger J, Forest S, Jeulin D and Colin C 2011 Homogenization of periodic auxetic materials *Procedia Eng.* **10** 1847–52
[14] Korner C and Liebold-Ribeiro Y 2015 A systematic approach to identify cellular auxetic materials *Smart Mater. Struct.* **24** 2

[15] Domaschke S, Morel A, Fortunato G and Ehret A E 2019 Random auxetics from buckling fibre networks *Nat. Commun.* **10** 4863
[16] Amjadi M, Pichitpajongkit A, Lee S, Ryu S and Park I 2014 Highly stretchable and sensitive strain sensor based on silver nanowire-elastomer nanocomposite *Acs Nano* **8** 5154–63
[17] Park J J, Hyun W J, Mun S C, Park Y T and Park O O 2015 Highly stretchable and wearable graphene strain sensors with controllable sensitivity for human motion monitoring *ACS Appl. Mater. Interfaces* **7** 6317–24
[18] Goodman S M *et al* 2021 Scalable manufacturing of fibrous nanocomposites for multifunctional liquid sensing *Nano Today* **40** 101270
[19] Zhang J Y, Goodman S M, Wise H G, Dichiara A B and Chung J H 2021 Electromechanical coupling of isotropic fibrous networks with tailored auxetic behavior induced by water-printing under tension *J. Mater. Chem.* **9** 4544–53
[20] Dichiara A B, Song A, Goodman S M, He D and Bai J 2017 Smart papers comprising carbon nanotubes and cellulose microfibers for multifunctional sensing applications *J. Mater. Chem.* **5** 20161–9
[21] Goodman Sheila M, Ferguson N and Dichiara A B 2017 Lignin-assisted double acoustic irradiation for concentrated aqueous dispersions of carbon nanotubes *RSC Adv.* **7** 5488–96
[22] Qi H S, Mader E and Liu J W 2013 Unique water sensors based on carbon nanotube-cellulose composites *Sens. Actuators B Chem.* **185** 225–30
[23] Zampetti E *et al* 2009 Design and optimization of an ultra thin flexible capacitive humidity sensor *Sens. Actuators B Chem.* **143** 302–7
[24] Kim J, Cho J-H, Lee H-M and Hong S-M 2021 Capacitive humidity sensor based on carbon black/polyimide composites *Sensors* **21** 1974
[25] Gu L, Huang Q-A and Qin M 2004 A novel capacitive-type humidity sensor using CMOS fabrication technology *Sens. Actuators B Chem.* **99** 491–8
[26] Boudaden J *et al* 2018 Polyimide-based capacitive humidity sensor *Sensors* **18** 1516
[27] Liu J *et al* 2011 *In situ* growth of continuous thin metal–organic framework film for capacitive humidity sensing *J. Mater. Chem.* **21** 3775–8
[28] Rauf S *et al* 2020 Highly selective metal–organic framework textile humidity sensor *ACS Appl. Mater. Interfaces* **12** 29999–30006
[29] Chappanda K N, Chaix A, Surya S G, Moosa B A, Khashab N M and Salama K N 2019 Trianglamine hydrochloride crystals for a highly sensitive and selective humidity sensor *Sens. Actuators B Chem.* **294** 40–7
[30] Steele J J, Fitzpatrick G A and Brett M J 2007 Capacitive humidity sensors with high sensitivity and subsecond response times *IEEE Sens. J.* **7** 955–6
[31] Gaspar C, Olkkonen J, Passoja S and Smolander M 2017 Paper as active layer in inkjet-printed capacitive humidity sensors *Sensors* **17** 1464
[32] Han KI *et al* 2017 Compliment graphene oxide coating on silk fiber surface via electrostatic force for capacitive humidity sensor applications *Sensors* **17** 407
[33] Hernández-Rivera D, Rodríguez-Roldán G, Mora-Martínez R and Suaste-Gómez E 2017 A capacitive humidity sensor based on an electrospun PVDF/graphene membrane *Sensors* **17** 1009
[34] Altenberend U *et al* 2013 Towards fully printed capacitive gas sensors on flexible PET substrates based on Ag interdigitated transducers with increased stability *Sens. Actuators B Chem.* **187** 280–7
[35] Li X Y, Chen XD, Chen X P, Ding X and Zhao X 2018 High-sensitive humidity sensor based on graphene oxide with evenly dispersed multiwalled carbon nanotubes *Mater. Chem. Phys.* **207** 135–40
[36] Boutros S and Hanna A A 1978 Dielectric properties of moist cellulose *J. Polym. Sci. A: Polym. Chem.* **16** 89–94
[37] Murphy E J 1929 Electrical conduction in textiles II Alternating current conduction in cotton and silk *J. Phys. Chem.* **33** 200–15